Manipulation of Goos-Hänchen shifts in the atomic configuration of mercury via interacting dark-state resonances

H. R. Hamedi,[1,*] Arash Radmehr,[2] and M. Sahrai[2,3]

[1]*Institute of Theoretical Physics and Astronomy, Vilnius University, A. Gostauto 12, LT-01108 Vilnius, Lithuania*

[2]*Research Institute for Applied Physics and Astronomy, University of Tabriz, Tabriz, Iran*

[3]*Photonics Excellence, University of Tabriz, Tabriz, Iran*

(Received 14 September 2014; revised manuscript received 28 October 2014; published 19 November 2014)

We study the manipulation of Goos-Hänchen (GH) shifts for the reflected and transmitted probe light pulses injected into a cavity containing four-level configuration mercury atoms where the probe transition is in the ultraviolet (UV) region with a wavelength of 253.7 nm. Different behaviors of the GH shifts can be observed in the absence, or presence, of two driving fields as well as an incoherent pump field. When neither coherent driving fields nor incoherent pumping is turned on, we realize negative reflected GH shifts for anomalous dispersion. Including only one driving field leads to subluminal-based light propagation with positive lateral shifts at certain incident angles. Taking into account the impact of both driving fields, negative GH shifts reappear in the reflected part of the incident light. The origin of this defect is attributed to interacting double dark resonances due to a high-resolution absorption peaks with a very steep negative slope of dispersion in the susceptibility profile. We then show that one can surpass this defect by applying a weak incoherent pumping field to obtain positive GH shifts for both reflected and transmitted light beams. Finally, using the $6\,^1P_1 \leftrightarrow 6\,^1S_0$ transition of Hg, we generalize our study to the case where the wavelength of the probe transition is 185 nm which is in the vacuum-ultraviolet domain. Although the number of oscillations is now increased, however, similar results are reported with respect to the case of UV transition.

DOI: 10.1103/PhysRevA.90.053836 PACS number(s): 42.25.Gy, 42.25.Bs, 42.50.Md

I. INTRODUCTION

Physical processes that could facilitate coherent control of light propagation have been an active area of research [1–4]. Recently, the study on slow and fast light is under active exploration due to its potential applications in optical signal processing and all-optical packet-switched networks [5,6]. Electromagnetically induced transparency (EIT), is a promising way that provides controlling the propagation velocity of optical pulses in the atomic medium with steep normal or anomalous dispersion (slow and fast light) [7,8]. EIT in coherently prepared atomic systems has led to dramatic new effects such as optical bistability (OB) [9–13], giant Kerr nonlinearity [14–17], four-wave mixing (FWM) [18], lasing without inversion [19,20], and large enhancement of the refractive index [21–23]. Enhancement of the refractive index without changing the structure leads to an interesting phenomenon, i.e., coherent control of the Goos-Hänchen (GH) shift.

The Goos-Hänchen effect [24] is an optical phenomenon in which a light beam experiences a lateral shift from the position predicted by geometrical optics, when totally reflected from a single interface between two different refraction media, one with a higher refractive index than the other [25].

Such lateral shift is attributed to the evanescent wave that travels along the interface. It occurs as if the incident light penetrates first into the medium with lower refractive index as an evanescent wave before being totally reflected back into the high-index medium. The GH shift plays a functional role in various fields of science such as micro-optics and nano-optics, acoustics, quantum and plasma physics [25], and in optical heterodyne sensors, which are employed to measure refractive index, displacement, temperature, beam angle, and film thickness [26]. Different structures are employed to explore the GH shift, such as photonic crystals [27], lossless dielectric slab [28], various-level configuration systems [29–35], negative refractive media [36], graphene [37–41], the ballistic electrons in semiconductor quantum slabs or wells [42,43], and so on [44–53]. For instance, Zubairy *et al.* [29,30] presented proposals to manipulate the Goos-Hänchen shift of a light beam via coherent control field, which is injected into a cavity configuration containing the two-level, three-level, or four-level atoms with EIT. The effect of quantum interference induced by incoherent pump and spontaneous emission upon the control of GH shifts is also discussed [32]. Abbas and colleagues investigated the influence of the Kerr nonlinearity on the group index of a dispersive intracavity medium through a Raman gain–based scheme to obtain amplitude control of GH shift in the reflected light [33]. They found that due to the presence of the Kerr field a relatively large positive or negative GH shift can be achieved.

In this paper we explore the behavior of GH shifts of a probe beam which is reflected from or transmitted through a cavity containing the four-level mercury atoms with fixed geometrical configuration. In particular, we investigate four different conditions. First, when the effect of driving fields and an incoherent pumping is neglected, we observe a large absorption under superluminal propagation of light. Simultaneously, the reflected part of incident light sustains negative GH shifts, while the transmitted light experiences positive GH shifts. Large positive lateral shifts can be obtained through proper adjusting of the first driving field, when the second driving field is off. Then we investigate the impact of

*Corresponding author: Hamid.R.Hamedi@gmail.com

the second driving field as well as a weak incoherent pumping rate on lateral shifts. We show that the lateral shifts will be dramatically modified, so that giant negative or positive GH shifts can be observed. This behavior is explained by the interacting dark resonances which can be justified by dressed-state analysis. Eventually, we study the behavior of GH shifts for both reflected and transmitted light beams when the wavelength of the probe transition is 185 nm located in the vacuum-ultraviolet (VUV) domain.

II. THEORY, MODEL, AND EQUATIONS OF THE MOTION

As shown in Fig. 1(a), a well-collimated transverse-electric (TE)-polarized probe light beam E_p having angular frequency ω_p is incident from vacuum ($\varepsilon_0 = 1$) upon the cavity at an angle θ from the normal. The incident medium is composed of two nonmagnetic dielectric slabs (ε_1) with identical thickness d_1 and the intracavity four-level atomic medium with thickness d_2. The atomic scheme consists of three atomic states ($|2\rangle, |3\rangle, |4\rangle$) in a ladder configuration, with an additional fourth perturbing state ($|1\rangle$) coupled by a laser field to the upper state of the ladder system as illustrated in Fig. 1(b). Transition $|1\rangle \leftrightarrow |4\rangle$ is driven by a coupling field with frequency ω_{41} and Rabi frequency Ω_{41}. A coherent driving field with frequency ω_{42} and the Rabi frequency Ω_{42} drives the transition $|2\rangle \leftrightarrow |4\rangle$, while a weak tunable probe field of frequency ω_{23} and Rabi frequency $\Omega_{23} = \Omega_p$ couples transition $|2\rangle \leftrightarrow |3\rangle$. Probe transition is also coupled by a weak incoherent driving field with pump strength R. The possible experimental candidate for this system is mercury (Hg) [54,55]. Relevant Hg levels are shown in Fig. 1(c), which is identical to that shown in Fig. 1(b) except for an additional level $6\,^3P_0$ labeled $|5\rangle$. Note that here, the probe transition is in the ultraviolet region with a low wavelength of 253.7 nm. We further include spontaneous decay from $|i\rangle$ to $|j\rangle$ ($i, j = 1,2,3,4$) with rate γ_{ij} on the dipole-allowed transitions. The atomic transition frequency is denoted by $\bar{\omega}_{ij}$, and the laser field detuning with respect to the atomic transition frequency is $\Delta_{ij} = \omega_{ij} - \bar{\omega}_{ij}$.

The corresponding Hamiltonian for the system under consideration is

$$H_I = \Delta_{23}|2\rangle\langle 2| + (\Delta_{42} + \Delta_{41})|4\rangle\langle 4| - (\Omega_p|2\rangle\langle 3| + \Omega_{41}|4\rangle\langle 1| + \Omega_{42}|4\rangle\langle 2| + \text{H.c.}). \quad (1)$$

The equation of motion of the density matrix is described by the Liouville equation:

$$\dot{\rho} = -\frac{i}{\hbar}[\text{H}, \rho] + L_\rho\,, \quad (2)$$

where L_ρ indicates the decay part of the system. By adopting the standard approach, the density-matrix equations of motion in dipole and rotating-wave approximations for this system

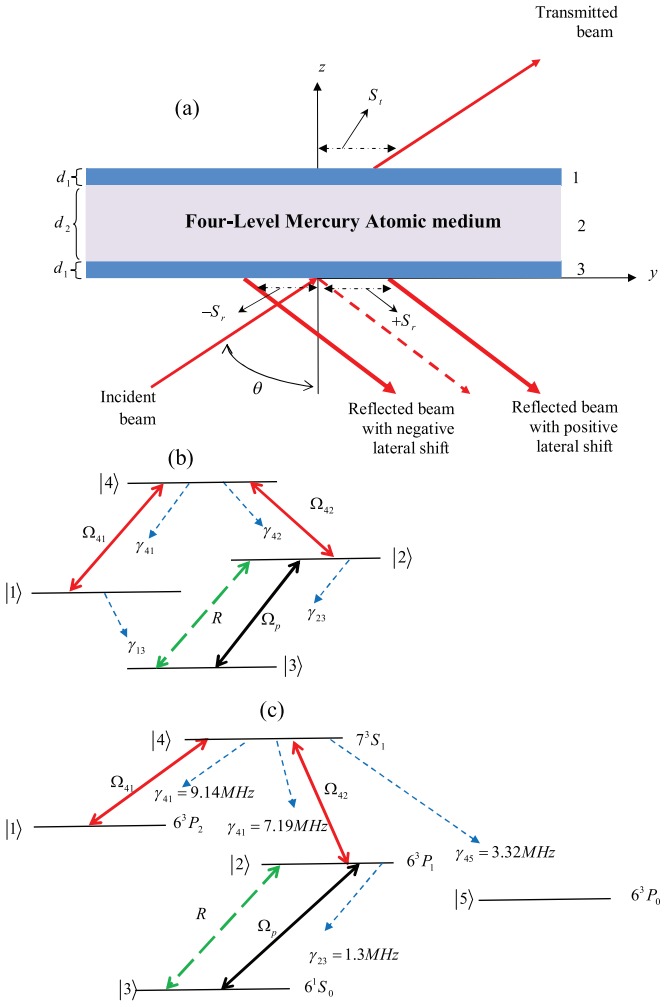

FIG. 1. (Color online) (a) Schematic of a cavity containing a four-level mercury atomic medium. (b) Schematic of a four-level atomic system. (c) Relevant energy levels of mercury when the probe transition is 253.7 nm. Population transfer to state $6\,^3P_0$ has to be compensated via a repump field.

can be written as follows:

$$\begin{aligned}
\dot{\rho}_{11} &= -2\gamma_{13}\rho_{11} + 2\gamma_{41}\rho_{44} - i\Omega_{41}^*\rho_{14} + i\Omega_{41}\rho_{41}\,,\\
\dot{\rho}_{22} &= -2\gamma_{23}\rho_{22} + 2\gamma_{42}\rho_{44} - 2R\rho_{22} + 2R\rho_{33} + i\Omega_p^*\rho_{32} - i\Omega_p\rho_{23} - i\Omega_{42}^*\rho_{24} + i\Omega_{42}\rho_{42},\\
\dot{\rho}_{33} &= 2\gamma_{13}\rho_{11} + 2\gamma_{23}\rho_{22} + 2R\rho_{22} - 2R\rho_{33} - i\Omega_p^*\rho_{32} + i\Omega_p\rho_{23}\,,\\
\dot{\rho}_{12} &= -(\Gamma_{12} + i\Delta_{41} - i\Delta_{42} + R)\rho_{12} - i\Omega_{42}^*\rho_{14} - i\Omega_p\rho_{13} + i\Omega_{41}\rho_{42}\,,\\
\dot{\rho}_{13} &= -(\Gamma_{13} + i\Delta_{41} - i\Delta_{42} - i\Delta_p + R)\rho_{13} - i\Omega_p^*\rho_{12} + i\Omega_{41}\rho_{43}\,,\\
\dot{\rho}_{14} &= -(\Gamma_{14} + i\Delta_{41})\rho_{14} - i\Omega_{41}\rho_{11} + i\Omega_{41}\rho_{44} - i\Omega_{42}\rho_{12}\,,\\
\dot{\rho}_{23} &= -(\Gamma_{23} - i\Delta_p + 2R)\rho_{23} - i\Omega_p^*\rho_{22} + i\Omega_p^*\rho_{33} + i\Omega_{42}\rho_{43}\,,\\
\dot{\rho}_{24} &= -(\Gamma_{24} + i\Delta_{42} + R)\rho_{24} - i\Omega_{42}\rho_{22} + i\Omega_{42}\rho_{44} + i\Omega_p^*\rho_{34} - i\Omega_{41}\rho_{21}\,,\\
\dot{\rho}_{34} &= -(\Gamma_{34} + i\Delta_p + i\Delta_{42} + R)\rho_{34} + i\Omega_p\rho_{24} - i\Omega_{41}\rho_{31} - i\Omega_{42}\rho_{32}\,,\\
\rho_{44} &= 1 - \rho_{11} - \rho_{22} - \rho_{33}\,.
\end{aligned} \quad (3)$$

In the above equations, $\Gamma_{ij} = (2\gamma_i + 2\gamma_j)/2$ are the damping rates of the coherences with γ_i being the total decay rate out of state $|i\rangle$, and $\Delta_p = \Delta_{23}$ is the detuning of the probe field.

The response of the atomic system to the applied fields is determined by the susceptibility, which is defined as

$$\chi(\omega_p) = \frac{N\wp_p}{\varepsilon_0 E_p}\rho_{23}(\omega_p)\,, \tag{4}$$

where N is the atom number density in the medium, $\wp_p$ is the probe transition dipole moment, and $\chi = \chi' + i\chi''$ is a complex quantity. The real and imaginary parts of χ correspond to the dispersion and the absorption of a weak probe field, respectively.

In order to drive the linear susceptibility we need to obtain the steady-state solution of the density-matrix equations. The general analytical solution for the coherence term ρ_{23} is

$$\rho_{23} = \frac{i\Omega_p\left(bc + \Omega_{41}^2\right)}{abc + c\Omega_{42}^2 + a\Omega_{41}^2}\,, \tag{5}$$

where

$$\begin{aligned} a &= \Gamma_{23} - i\Delta_p + 2R \\ b &= \Gamma_{34} - i\Delta_p - i\Delta_{42} + R, \\ c &= \Gamma_{13} + i\Delta_{41} - i\Delta_{42} - i\Delta_p + R. \end{aligned} \tag{6}$$

Upon inserting Eq. (5) into Eq. (4), the susceptibility of the intracavity medium can be easily calculated. From the well-known relation $\varepsilon_2 = 1 + \chi$, it is obvious that susceptibility of the intracavity medium is frequency dependent and can be manipulated by using the coherent control of the driving fields as well as incoherent pump field to get superluminal or subluminal light propagation.

It is known that when a weak probe field is applied to the transition $|2\rangle \leftrightarrow |3\rangle$, the group velocity is defined by $v_g = c/n_g$ with n_g and c being the group refractive index and vacuum light speed, respectively. The group velocity depends on susceptibility χ_{23} for the transition $|2\rangle \leftrightarrow |3\rangle$ and its rate change is as follows [33]:

$$n_g = 1 + \frac{1}{2}\chi'_{23} + \frac{1}{2}\omega_p\frac{\partial\chi'_{23}}{\partial\omega_p}\,, \tag{7}$$

where χ'_{23} is the real part of χ_{23}.

It is instructive to study the dependence of the GH shifts upon the group index of the cavity corresponding to superluminal and subluminal light propagation. To explore the behavior of the group index corresponding to the total cavity which includes the walls of the cavity and the atomic medium inside the cavity, we consider that the cavity consists of three layers (as mentioned previously); layers 1 and 3 are the walls of the cavity with thickness $d_1 = 0.2\ \mu$m each, and layer 2 is the intracavity medium with thickness $d_2 = 5\ \mu$m. Therefore, the total width or thickness of the cavity is $L = 2d_1 + d_2$. The group index of the cavity can be calculated by using the relation between the group velocity v_g and the group delay τ_g.The expression for the group velocity corresponding to the reflected or transmitted light beam is given by

$$v_g^{r,t} = \frac{L}{\tau_g^{r,t}}\,, \tag{8}$$

where the superscripts r,t correspond to reflection and transmission parts of the incident light beam. The corresponding group delay of the cavity can be written as

$$\tau_g^{r,t} = \frac{\partial\varphi_{r,t}}{\partial\omega_p}\,. \tag{9}$$

Moreover, the group index, defined as the ratio of the speed of light in vacuum to the group velocity $v_g^{r,t}$ of both reflected and transmitted probe light beam can be approximated as

$$N_g^{r,t} = c/v_g^{r,t} \approx \frac{1}{L}\frac{d\varphi_{r,t}}{d\omega_p}. \tag{10}$$

This shows that the group index of the cavity depends on the thickness of the cavity L and the derivative (with respect to probe light frequency) of the phase associated with the reflected or the transmitted probe light beam, and positive or negative GH shift can be realized by changing the group index $N_g^{r,t}$ to positive or negative values, respectively.

Using a standard characteristic matrix approach we can easily calculate the amplitude transmission $T(k_y,\omega_p)$ and reflection $R(k_y,\omega_p)$ for the weak probe light beam passing through the cavity at a given frequency ω_p:

$$M_j(k_y,\omega_p,d_j) = \begin{pmatrix} \cos\left[k_z^j d_j\right] & i\sin\left[k_z^j d_j\right]/q_j \\ iq_j\sin\left[k_z^j d_j\right] & \cos\left[k_z^j d_j\right] \end{pmatrix}, \tag{11}$$

where M_j is the transfer matrix of the jth layer ($j = 1,2,3$), $k_z^j = \sqrt{\varepsilon_j k^2 - k_y^2}$ denotes the z component of the wave number in the jth layer, $q_j = k_z^j/k$, d_j shows the thickness of the jth layer, k_y represents the y component of the wave number ($k = \omega_p/c$) in vacuum, and c is the light speed in vacuum. The total transfer matrix for the considering cavity is given by

$$Q(k_y,\omega_p) = M_1(k_y,\omega_p,d_1)M_2(k_y,\omega_p,d_2)M_3(k_y,\omega_p,d_1)\,. \tag{12}$$

Therefore Fresnel equations for the reflection R and transmission T are

$$R(k_y,\omega_p) = \frac{q_0(Q_{22} - Q_{11}) - \left(q_0^2 Q_{12} - Q_{21}\right)}{q_0(Q_{22} + Q_{11}) - \left(q_0^2 Q_{12} + Q_{21}\right)}, \tag{13a}$$

$$T(k_y,\omega_p) = \frac{2q_0}{q_0(Q_{22} + Q_{11}) - \left(q_0^2 Q_{12} + Q_{21}\right)}, \tag{13b}$$

where $q_0 = k_0/k$ and Q_{ij} are the elements of matrix $Q(k_y,\omega_p)$.

With the assumption of a well-collimated probe light beam with a sufficiently large width (i.e., with a narrow angular spectrum, $\Delta k \ll k$), and according to the stationary-phase approach, and after denoting the reflection and transmission coefficients $R = |R|\,e^{i\varphi_r}$ and $T = |T|\,e^{i\varphi_t}$, respectively, the longitudinal lateral shift known as Goos-Hänchen shift for both reflected and transmitted beams can be estimated as

$$S_{r,t} = -\frac{\lambda}{2\pi}\frac{d\varphi_{r,t}}{d\theta}, \tag{14}$$

where $\varphi_{r,t}$ are the phases of $R(k_y,\omega_p)$ and $T(k_y,\omega_p)$.

As a result, the lateral or GH shift in the reflected and transmitted probe light beams can be expressed as

$$S_r = -\frac{\lambda}{2\pi|X|^2}\left\{\mathrm{Re}[X_r]\frac{d\mathrm{Im}[X_r]}{d\theta} - \mathrm{Im}[X_r]\frac{d\mathrm{Re}[X_r]}{d\theta}\right\}, \tag{15a}$$

$$S_t = -\frac{\lambda}{2\pi|X_t|^2}\left\{\mathrm{Re}[X_t]\frac{d\mathrm{Im}[X_t]}{d\theta} - \mathrm{Im}[X_t]\frac{d\mathrm{Re}[X_t]}{d\theta}\right\}, \tag{15b}$$

where $X_r = r(k_y,\omega_p)$ and $X_t = t(k_y,\omega_p)$.

III. RESULTS AND DISCUSSION

In the following, we analyze in detail the behavior of the GH shifts of the transmitted and reflected probe beams by using the numerical result from the density-matrix equation of motions ρ_{ij}. Now we start to investigate the GH shift patterns from different respects, i.e., (case III A): both driving lasers Ω_{41},Ω_{42} as well as the incoherent pumping R are off ($\Omega_{41} = \Omega_{42} = R = 0$); (case III B): only Ω_{42} is turned on, but Ω_{41} and R are off ($\Omega_{42} \neq 0, \Omega_{41} = R = 0$); (case III C): both Ω_{41} and Ω_{42} are now on, but R is still off ($\Omega_{41} \neq 0, \Omega_{42} \neq 0, R = 0$); and finally (case III D): all the driving fields and the incoherent pump field are turned on($\Omega_{41} \neq 0, \Omega_{42} \neq 0, R \neq 0$).

For this article, the ratios of the decay rates are $\gamma_{41} = \gamma$, $\gamma_{42} = 0.79\gamma$, $\gamma_{23} = 0.14\gamma$, [54,55] which correspond to the case found in mercury [Fig. 1(c)]. For cases III A and III B, a weak decay rate $\gamma_{13} = 0.01\gamma$ is considered to avoid the population to be trapped in state $|1\rangle$ in the steady-state case. In addition, in both cases III C and III D we neglect the decay on transition $|1\rangle \leftrightarrow |3\rangle$ ($\gamma_{13} = 0$), which is because the trapping in state $|1\rangle$ is now avoided due to the existence of an additional laser field Ω_{41}. Note that in the following all the parameters are in the units of $\gamma_{41} = \gamma = 9.14$ MHz corresponding to the decay rate along the $|1\rangle \leftrightarrow |4\rangle$ transition of the mercury system.

A. The case $\Omega_{41} = \Omega_{42} = R = 0$

Firstly, we start to analyze the lateral shifts for the reflected and transmitted probe beams in the absence of both driving fields Ω_{41} and Ω_{42}. Also, in this case the rate of incoherent pumping R is considered to be zero. Dropping Ω_{41}, Ω_{42}, and R, Eqs. (5) and (6) become

$$\rho_{23} = -i\Omega_p\frac{\Delta_p^2 + i\Delta_p(\gamma_{13}+\gamma_{41}+\gamma_{42}) - \gamma_{13}(\gamma_{41}+\gamma_{42})}{d}, \tag{16}$$

with

$$d = i\Delta_p^3 - \Delta_p^2[\gamma_{41}+\gamma_{42}+\gamma_{13}+\gamma_{23}] - i\Delta_p[\gamma_{13}\gamma_{23}+\gamma_{13}\gamma_{41}+\gamma_{13}\gamma_{42}+\gamma_{23}\gamma_{41}+\gamma_{23}\gamma_{42}]. \tag{17}$$

In this case, as is known, the system changes to a two-level absorber atomic system with no dark states, accompanied with superluminal light propagation inside the intracavity medium. This condition can be seen in Fig. 2(a), when we display the linear susceptibility of the atomic medium versus Δ_p.The corresponding plot of the GH shift in the reflected and transmitted probe light beams versus incident angle θ ranging from 0 to $\pi/2$ is shown in Fig. 2(b). As it is expected, a negative shift occurs for the reflected probe beam, while the transmitted probe beam experiences the positive shift [29–34].

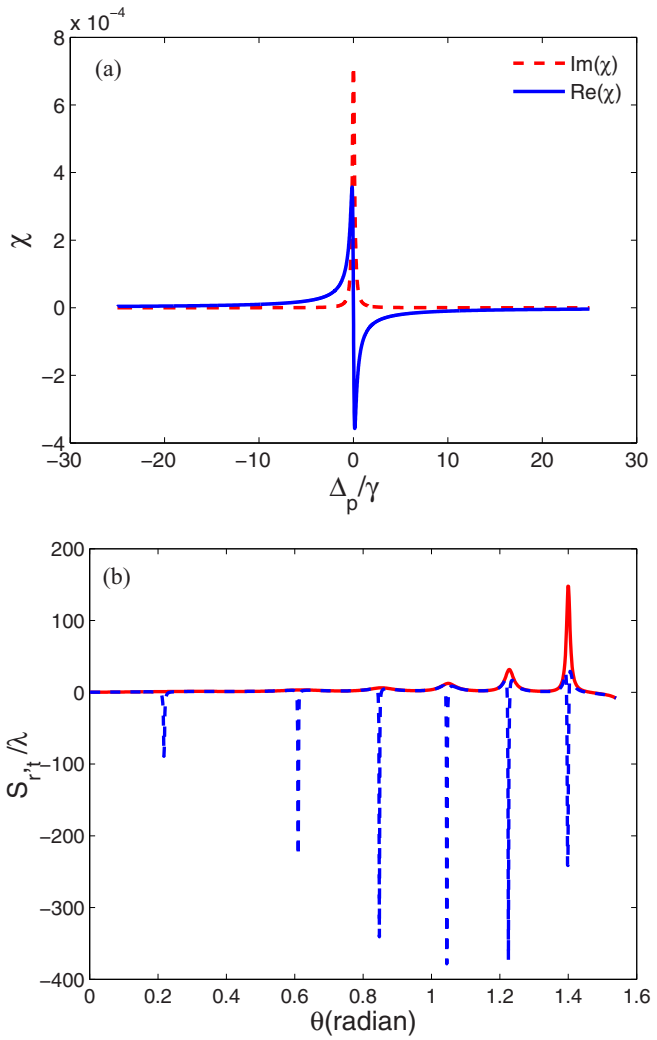

FIG. 2. (Color online) (a) Probe absorption and dispersion versus probe field detuning. (b) Lateral shifts S_r and S_t at different incident angles ranging from 0 to $\pi/2$. The selected parameters are $\gamma_{41} = \gamma = 9.14$ MHz, $\Omega_p = 10^{-4}\gamma$, $\Omega_{41} = \Omega_{42} = R = 0$, $\Delta_{41} = \Delta_{42} = 0$, $\gamma_{41} = \gamma$, $\gamma_{42} = 0.79\gamma$, $\gamma_{23} = 0.14\gamma$, and $\gamma_{13} = 0.01\gamma$. For (b) $\Delta_p = 0$, $d_1 = 0.2\,\mu$m, $d_2 = 5\,\mu$m, $\varepsilon_0 = 1$, $\lambda_{23} = 253.7$ nm.

B. The case $\Omega_{42} \neq 0$, $\Omega_{41} = R = 0$

In Ref. [56], Wang and colleagues demonstrated the existence of a large negative shift near resonance due to the weak absorption of the dielectric slab. Nevertheless, the lateral shifts of the reflected and transmitted beams cannot be manipulated once one chooses the structure [27,28,47,56–58]. However, it is already shown that the dispersive-absorptive

properties of the intracavity medium can dramatically modify the resonant conditions of the cavity system [29]. Hence in this proposal we expect that the lateral shifts of the reflected and transmitted probe beams can be easily manipulated by suitable regulating the intensity of applied field.

When only the driving field Ω_{42} is turned on, Eqs. (5) and (6) find the form

$$\rho_{23} = -i\Omega_p \frac{\Delta_p^2 + i\Delta_p(\gamma_{13}+\gamma_{41}+\gamma_{42}) - \gamma_{13}(\gamma_{41}+\gamma_{42})}{e}, \tag{18}$$

and

$$\begin{aligned} e = {} & i\Delta_p^3 - \Delta_p^2[\gamma_{41}+\gamma_{42}+\gamma_{13}+\gamma_{23}] \\ & - i\Delta_p\big[\Omega_{42}^2 + \gamma_{13}\gamma_{23} + \gamma_{13}\gamma_{41} \\ & + \gamma_{13}\gamma_{42} + \gamma_{23}\gamma_{41} + \gamma_{23}\gamma_{42}\big] + \gamma_{13}\Omega_{42}^2. \end{aligned} \tag{19}$$

Obviously, control field Ω_{42} can modify the optical susceptibility of the atomic sample [see Eqs. (18) and (19)]. So, according to Eqs. (11)–(15), we expect controllable GH shifts for the reflected and transmitted probe beams through adjusting the driving field Ω_{42}.

Typical probe absorption-dispersion curves are plotted in Fig. 3. It is realized that for $\Omega_{42} = 8\gamma$ (and $\Omega_{41} = R = 0$) the central strong absorption peak observed in Fig. 2(a) splits completely, so that two absorption peaks appear in both sides of zero probe detuning [Fig. 3(a)], leading to two Autler-Townes dressed components [see further Eq. (21)]. In this case, the absorption will be decreased at the line center of probe detuning and an EIT window appears. Moreover, the slope of dispersion changes to positive at $\Delta_p = 0$, suggesting subluminal propagation of light. Now we increase the intensity of Ω_{42} to 20γ. Figure 3(b) indicates that the restoration of dispersion slope to negative is not possible anymore by further increasing the intensity of Ω_{42}. However, the positions of the absorption peaks move away from zero detuning.

The corresponding lateral shifts of the reflected and transmitted probe light beams for incident angle are displayed in Fig. 4. It is easy to find that when $\Omega_{42} = 8\gamma$, both S_r and S_t demonstrate giant positive shifts at certain incident angles [Fig. 4(a)]. Moreover, although increasing Ω_{42} cannot change the positive sign of lateral shifts for reflected beam to negative, it leads to noticeable variations in magnitude of GH shift profiles at certain angles. Therefore, we observe the slow light-based condition accompanying with EIT being established leading to giant positive GH shifts in the reflected and transmitted probe beams at resonance. In fact, the cavity will undergo positive group index for the reflected and transmitted lights at certain incident angles which are computable through the relation $N_g \approx L^{-1}\frac{d\varphi_{r,t}}{d\omega_p}$ [30].

The reason for such a switch in the sign of GH shifts in the reflected probe beam can be interpreted deeper through the dressed-state picture which is discussed elsewhere [55]. In the absence of incoherent pumping ($R = 0$), the dressed eigenstates generated by the driving fields Ω_{42} and Ω_{41}

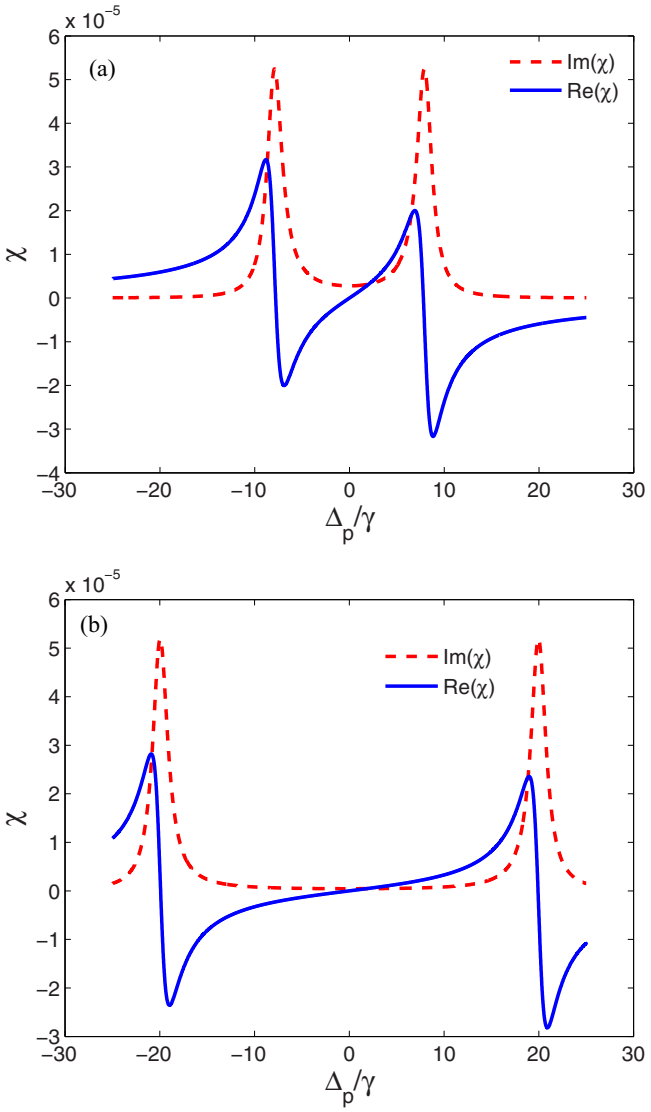

FIG. 3. (Color online) Probe absorption and dispersion versus probe field detuning. The selected parameters are (a) $\Omega_{42} = 8\gamma$, (b) $\Omega_{42} = 20\gamma$. The other parameters are the same as in Fig. 2.

read [55]

$$|d_1\rangle = \frac{1}{\sqrt{2\left(\Omega_{41}^2+\Omega_{42}^2\right)}}[\Omega_{41}|1\rangle + \Omega_{42}|2\rangle] + \frac{1}{\sqrt{2}}|4\rangle, \tag{20a}$$

$$|d_2\rangle = \frac{1}{\sqrt{\Omega_{41}^2+\Omega_{42}^2}}[\Omega_{41}|2\rangle - \Omega_{42}|1\rangle], \tag{20b}$$

$$|d_1\rangle = \frac{1}{\sqrt{2\left(\Omega_{41}^2+\Omega_{42}^2\right)}}[\Omega_{41}|1\rangle + \Omega_{42}|2\rangle] - \frac{1}{\sqrt{2}}|4\rangle, \tag{20c}$$

with the corresponding eigenenergies $E_3 = -E_1 = \hbar\sqrt{\Omega_{41}^2+\Omega_{42}^2}$ and $E_2 = 0$.

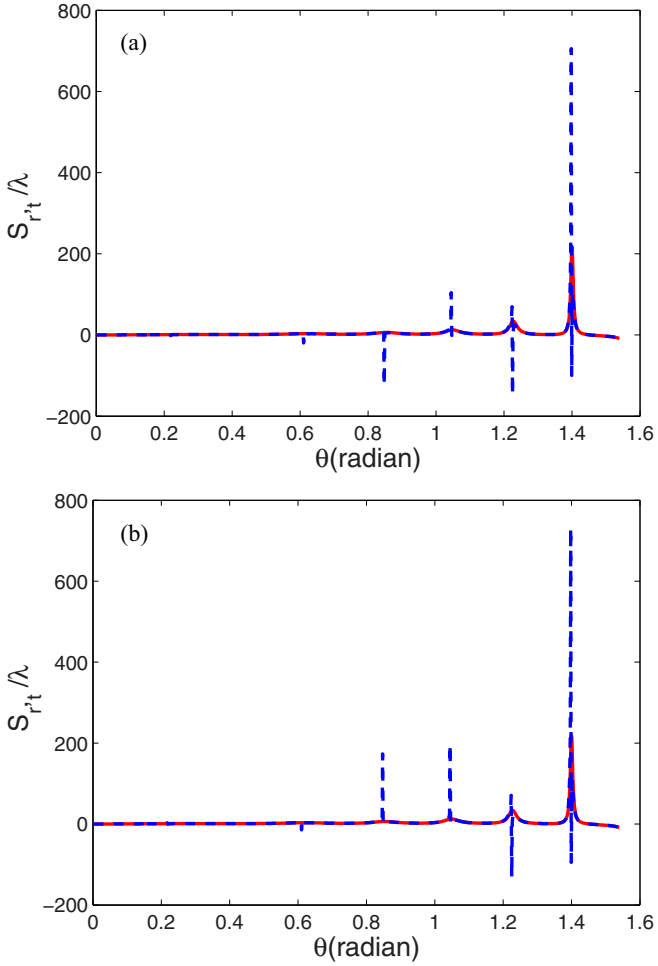

FIG. 4. (Color online) Lateral shifts S_r and S_t at different incident angles ranging from 0 to $\pi/2$. The selected parameters are (a) $\Omega_{42} = 8\gamma$, (b) $\Omega_{42} = 20\gamma$. The other parameters are the same as in Fig. 2.

Considering $\Omega_{41} = 0$, and for the strong driving field Ω_{42}, the set of Eq. (20) changes to

$$|d_1\rangle = \frac{1}{\sqrt{2}}|2\rangle + \frac{1}{\sqrt{2}}|4\rangle, \tag{21a}$$

$$|d_2\rangle = |1\rangle, \tag{21b}$$

$$|d_3\rangle = \frac{1}{\sqrt{2}}|2\rangle - \frac{1}{\sqrt{2}}|4\rangle, \tag{21c}$$

which means in the limit $\Omega_{41} = 0$, the second dressed state $|d_2\rangle$ will coincide with the bare state $|1\rangle$ and thus will be decoupled from the fields. In this case, two dressed states $|d_1\rangle$ and $|d_3\rangle$ with the splitting energy $2\hbar\Omega_{42}$ can be attributed to the usual Autler-Townes dressed components, corresponding to two peaks in the absorption profile in Fig. 3.

Now, we are interested in the signature of the thickness of the intracavity medium (d_2), on the behavior of the GH shifts $S_{r,t}$. It is known that the lateral shifts are very sensitive to the thickness of the cavity [28,56,59,60]. Zubairy *et al.* [30] showed that as one decreases the thickness of the intracavity medium, the number of oscillation peaks and dips will be reduced. However, the overall behavior of the reflected and transmitted beams will not alter. Now we plot the GH shifts

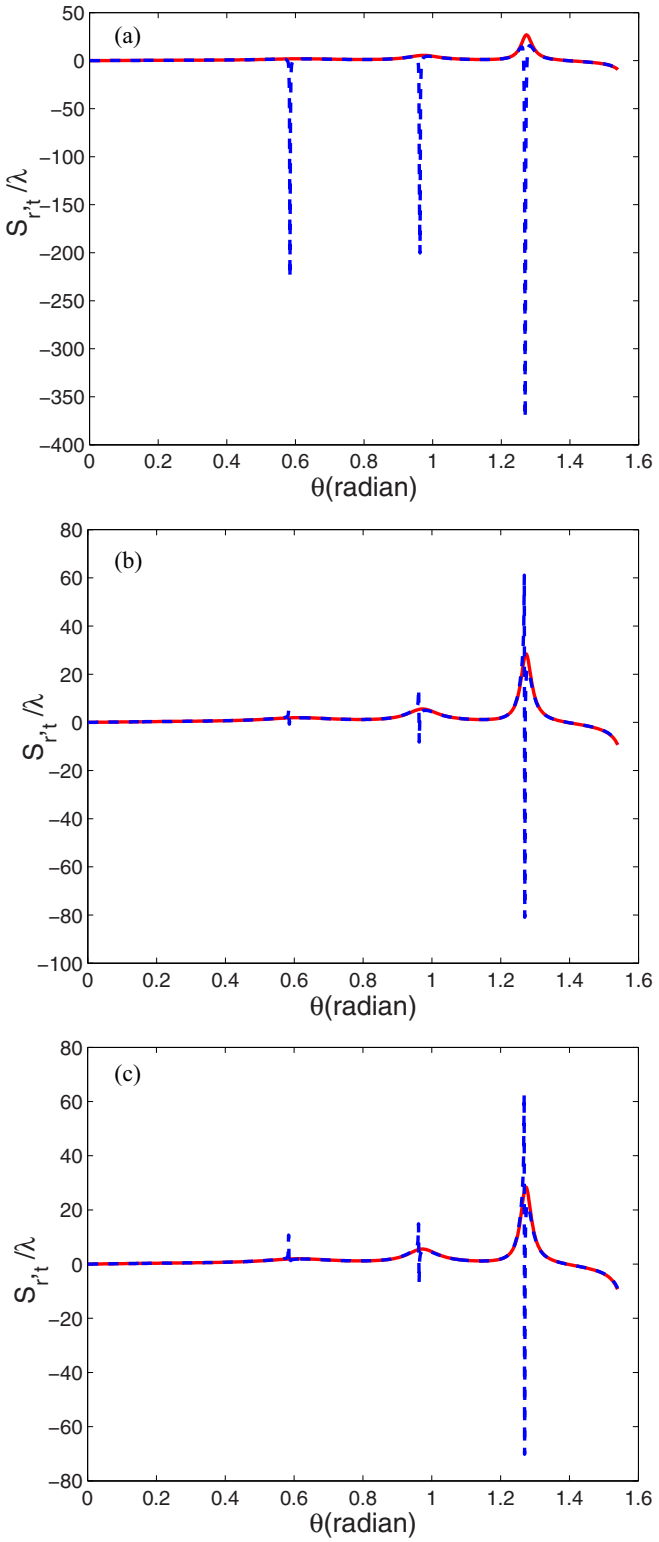

FIG. 5. (Color online) Lateral shifts S_r and S_t at different incident angles ranging from 0 to $\pi/2$. The selected parameters are $d_2 = 3$ μm, (a) $\Omega_{42} = 0$, (b) $\Omega_{42} = 20\gamma$, (c) $\Omega_{42} = 20\gamma$. The other parameters are the same as in Fig. 2.

in the reflected and transmitted light beams versus θ and for the same values of parameters as Figs. 2(b), 3(a), and 3(b). In this case, the thickness d_2 of the intracavity is decreased from $d_2 = 5$ μm to $d_2 = 3$ μm. Figure 5 illustrates that as it

is expected, the reduction on the thickness of the intracavity leads to a noticeable change in the number of oscillations in both the reflected and transmitted GH shifts. Moreover, the similar behavior of lateral shifts with our earlier results can be observed.

C. The case $\Omega_{41} \neq 0$, $\Omega_{42} \neq 0$, $R = 0$

Next, we turn to study the dependence of the lateral shifts on the incident angle of the probe beam for the case where we include the effect of perturbing field Ω_{41}, but still neglect the influence of incoherent pumping R. For this case, Eqs. (5) and (6) take the form

$$\rho_{23} = -i\Omega_p \frac{\Omega_{41}^2 + \Delta_p^2 + i\Delta_p(\gamma_{41} + \gamma_{42})}{f}, \tag{22}$$

with

$$f = i\Delta_p^3 - \Delta_p^2[\gamma_{41} + \gamma_{42} + \gamma_{23}] - i\Delta_p\left[\Omega_{41}^2 + \Omega_{42}^2 + \gamma_{23}\gamma_{41} + \gamma_{23}\gamma_{42}\right] + \gamma_{23}\Omega_{41}^2,. \tag{23}$$

In this case, the interacting dark resonances will be established.

The behavior of GH shifts of the reflected and transmitted probe beams as well as the susceptibility spectra are depicted in Fig. 6 in the presence of driving field Ω_{41}. We plot the curves for the case of $\Omega_{41} = \Omega_{42} = 8\gamma$. The results can be compared with Sec. III B, Figs. 3(a) and 4(a). We notice a strong influence of the Ω_{41} on the magnitude of GH shift for both the reflected and the transmitted light beams as shown in Fig. 6(a). In this condition, the reflected light experiences negative lateral shift for the whole range 0 to $\pi/2$, whereas the GH shift for the transmitted light in this range of angles is still positive. According to these results we may expect anomalous dispersion regions for the propagated light through the medium [33,34]. Let us now consider the behavior of linear susceptibility versus Δ_p for the given values of Fig. 6(a). Investigation on Fig. 6(b) shows that there exist three absorption peaks in the susceptibility profile; a very strong spikelike peak located at the line center of the absorption, as well as two weak absorption peaks in both the left and right sides of the central peak. Obviously, the slope of dispersion is negative again at $\Delta_p = 0$ which represents the superluminal condition. As a matter of fact, in the presence of Ω_{41}, the dressed states are ($\Omega_{41} = \Omega_{42} = \Omega$)

$$|d_1\rangle = \frac{1}{2}[|1\rangle + |2\rangle] + \frac{1}{\sqrt{2}}|4\rangle, \tag{24a}$$

$$|d_2\rangle = \frac{1}{2}[|2\rangle - |1\rangle], \tag{24b}$$

$$|d_1\rangle = \frac{1}{2}[|1\rangle + |2\rangle] - \frac{1}{\sqrt{2}}|4\rangle, \tag{24c}$$

and the eigenenergies are $E_3 = -E_1 = \sqrt{2}\hbar\Omega$, $E_2 = 0$. Three different eigenenergies are obtained yielding to three absorption peaks in the absorption profile [Fig. 6(b)]. This is due to the origin of the phenomenon of interacting double dark states.

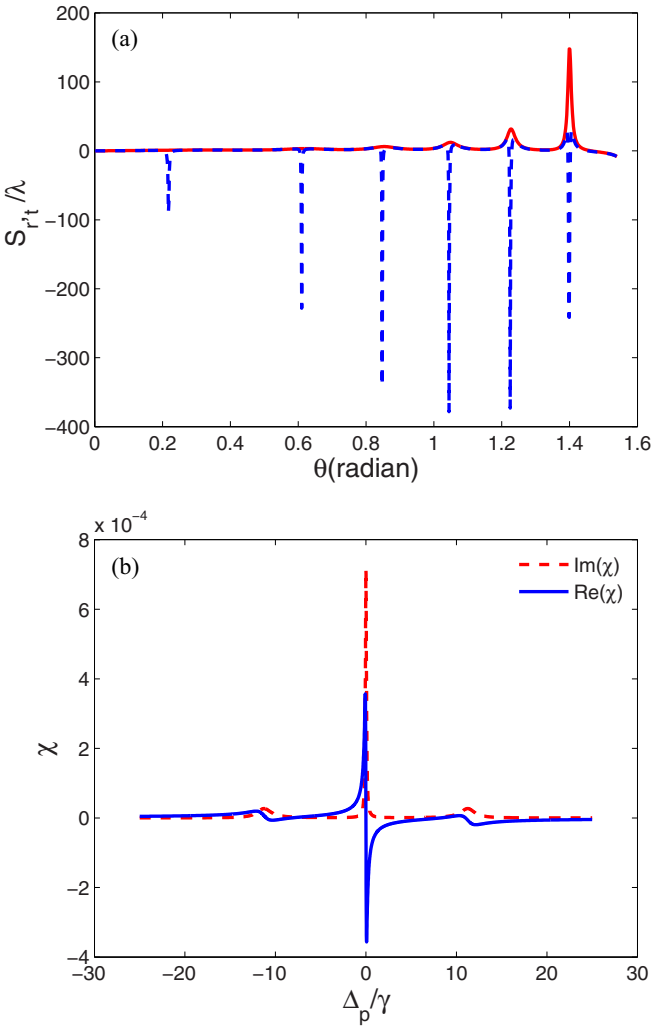

FIG. 6. (Color online) (a) Lateral shifts S_r and S_t at different incident angles ranging from 0 to $\pi/2$. (b) Probe absorption and dispersion versus probe field detuning. The selected parameters are $\Omega_{41} = \Omega_{42} = 8\gamma$ and $\gamma_{13} = R = 0$. The other parameters are the same as in Fig. 2.

D. The case $\Omega_{41} \neq 0$, $\Omega_{42} \neq 0$, $R \neq 0$

In this section, we analyze numerically whether the lateral shifts can be controlled or not when considering the effect of incoherent pumping field acting on the transition $|2\rangle \leftrightarrow |3\rangle$. After some algebraic calculations, the density-matrix element ρ_{23} of Eqs. (5) and (6) reads

$$\rho_{23} = -i\Omega_p \frac{\Omega_{41}^2 + \Delta_p^2 + i\Delta_p(\gamma_{13} + \gamma_{41} + \gamma_{42} + 2R) - R(\gamma_{41} + \gamma_{42}) + R^2}{h}, \tag{25}$$

and

$$h = i\Delta_p^3 - \Delta_p^2[\gamma_{41} + \gamma_{42} + \gamma_{23} + 4R] - i\Delta_p\left[\Omega_{41}^2 + \Omega_{42}^2 + \gamma_{23}\gamma_{41} + \gamma_{23}\gamma_{42} + R^2 + 3R(\gamma_{41} + \gamma_{42}) + 2R\gamma_{23} + 4R\right] + 2R^3 + R^2[2\gamma_{41} + 2\gamma_{42} + \gamma_{23}] + R\left[\gamma_{23}\gamma_{41} + \gamma_{23}\gamma_{42} + 2\Omega_{41}^2 + \Omega_{42}^2\right] + \gamma_{23}\Omega_{41}^2. \tag{26}$$

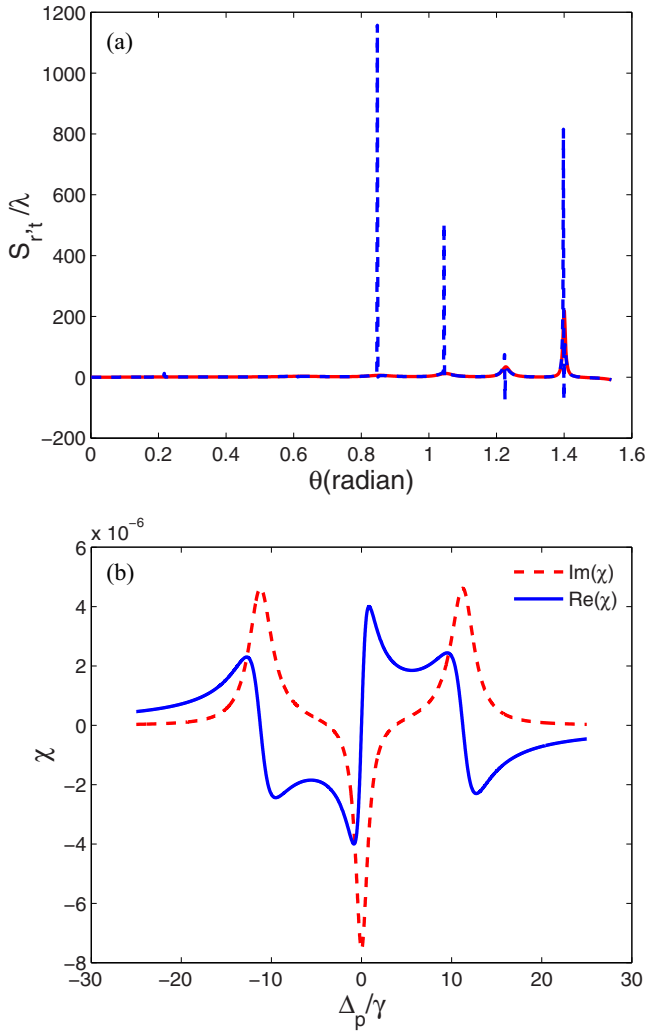

FIG. 7. (Color online) (a) Lateral shifts S_r and S_t at different incident angles ranging from 0 to $\pi/2$. (b) Probe absorption and dispersion versus probe field detuning. The selected parameters are $\Omega_{41} = \Omega_{42} = 8\gamma$, $\gamma_{13} = 0$, and $R = 0.5\gamma$. The other parameters are the same as in Fig. 2.

We plot the dependence of the S_r and S_t on the incoherent pumping rate R. The selected parameters are the same as in Fig. 6, except for $R = 0.5\gamma$. It is shown in Fig. 7(a) that GH shifts become positive and enhance dramatically with respect to Fig. 6(a). Figure 7(b) shows that the central peak in the presence of weak incoherent pumping becomes gain, and the slope of dispersion switches to positive showing normal dispersion, which leads to giant positive lateral shifts. Therefore, a powerful way is presented to control the susceptibility in order to manipulate the lateral shifts by using the incoherent pumping field.

Thus it is easily shown that one can control and even modify the lateral shifts through proper tuning of the driving fields and incoherent pumping rate. This controllability of the GH shifts on controlling parameters of the mercury atomic configuration is because of the dependence of the linear susceptibility of the intracavity medium to parameters Ω_{41}, Ω_{42}, and R. In fact, the variation in these parameters

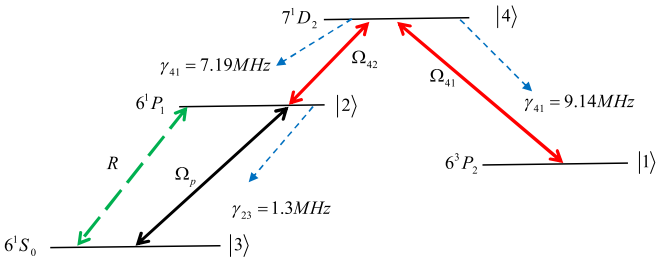

FIG. 8. (Color online) Relevant energy levels of mercury when the probe transition is 185 nm.

modifies the linear susceptibility of the cavity which leads the manipulation effects on the GH shifts.

As mentioned, we considered the mercury atomic system with probe resonance transition wavelength of 253.7 nm. Although this transition is not in the VUV region, it is a useful transition for practical applications. Fry *et al.* [54] have shown that by using a very similar scheme, it is possible to modify this four-level mercury to lase at wavelength of 185 nm by using the $6\,^1P_1 \leftrightarrow 6\,^1S_0$ transition of Hg which is in the VUV domain (Fig. 8). So, it would be worthwhile if we could also analyze the behavior of GH shifts where the probe transition is now in the VUV domain with a probe transition wavelength of 185 nm. For this purpose, we plot the lateral shifts against incident angles in Fig. 9 for four different parametric conditions discussed in Secs. III A–III D, i.e., (a) $\Omega_{41} = \Omega_{42} = R = 0$, $\gamma_{13} = 0.01\gamma$, (b) $\Omega_{42} = 8\gamma$, $\Omega_{41} = R = 0$, $\gamma_{13} = 0.01\gamma$, (c) $\Omega_{41} = \Omega_{42} = 8\gamma$, $R = 0$, $\gamma_{13} = 0$, and (d) $\Omega_{41} = \Omega_{42} = 8\gamma$, $R = 0.5\gamma$, $\gamma_{13} = 0$. We find that the behavior of lateral shifts for both reflected and transmitted beams are very similar to our previous results, so that both negative and positive GH shifts can be observed by proper tuning of the system parameters. However, it is shown that for this case, the number of oscillations increases with respect to our previous results shown in Figs. 2–7.

IV. GH SHIFTS IN A REAL SYSTEM

Up to now, we have demonstrated the GH shifts analysis based on the stationary-phase theory [61], so that the incident probe beam is considered as a plane wave. Our aim is now to show that for a real system when the incident wave has a Gaussian profile with finite width, our previous results will not be violated. This analysis is widely discussed already in detail in other works [29,34,62]. We follow the similar approach as already used in Refs. [29,34,47] to simulate the propagation of the weak Gaussian-shaped probe beam passing through the cavity containing the four-level mercury atoms. For the incident probe beam, the electric field at the plane $z = 0$ can take the integral form

$$E_x^i(y)|_{z=0} = (2\pi)^{-1/2} \int S(k_y) \exp(ik_y y) dk_y, \qquad (27)$$

with the initial angular spectrum of the Gaussian probe beam as

$$S(k_y) = \frac{w_y}{\sqrt{2}} \exp\left[-w_y^2 (k_y - k_{y0})^2/4\right], \qquad (28)$$

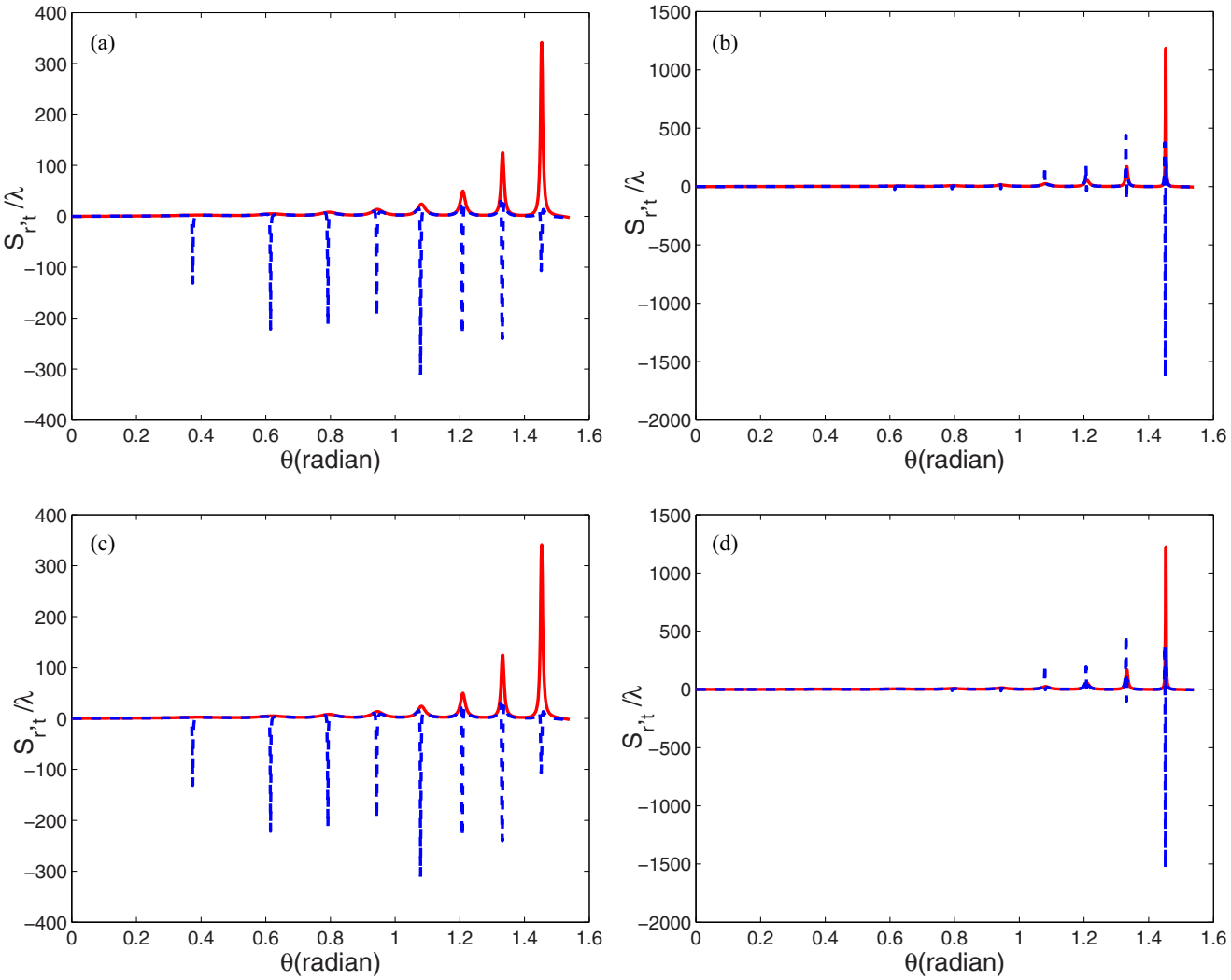

FIG. 9. (Color online) Lateral shifts S_r and S_t at different incident angles ranging from 0 to $\pi/2$. The selected parameters are $\lambda_{23} = 185$ nm. (a) $\Omega_{41} = \Omega_{42} = R = 0$, $\gamma_{13} = 0.01\gamma$; (b) $\Omega_{42} = 8\gamma$, $\Omega_{41} = R = 0$, $\gamma_{13} = 0.01\gamma$; (c) $\Omega_{41} = \Omega_{42} = 8\gamma$, $R = 0$, $\gamma_{13} = 0$; (d) $\Omega_{41} = \Omega_{42} = 8\gamma$, $R = 0.5\gamma$, $\gamma_{13} = 0$. The other parameters are the same as in Fig. 2.

and $k_{y0} = k\sin\theta$, $w_y = w\sec\theta$, where θ and w are the incident angle as well as the half-width of the probe beam at the incident plane of $z = 0$, respectively. The reflected and transmitted probe beams then read using Eq. (13),

$$E_x^r(y)|_{z=0} = (2\pi)^{-1/2}\int R(k_y,\omega_p)S(k_y)\exp(ik_y y)dk_y, \tag{29}$$

and

$$E_x^t(y)|_{z=2d_1+d_2} = (2\pi)^{-1/2}\int T(k_y,\omega_p)S(k_y)\exp(ik_y y)dk_y. \tag{30}$$

In this case, the initial angular spectrum distribution will be distributed sharply around k_{y0}. Following Fig. 8, we consider the $6\,^1P_1 \leftrightarrow 6\,^1S_0$ transition of Hg which is in the VUV domain ($\lambda_p = 185$ nm), so we can compare our simulations with the lateral shifts observed in Fig. 9. The plots of normalized intensity profiles of the incident (solid line), reflected (dashed line), and transmitted (dotted line) probe beams for $\theta = 1.2$ rad are given in Fig. 10 for two cases when $\Omega_{41} = \Omega_{42} = R = 0$, $\gamma_{13} = 0.01\gamma$, and $\Omega_{42} = 8\gamma$, $\Omega_{41} = R = 0$, $\gamma_{13} = 0.01\gamma$. Thus, our results will be comparable with Figs. 9(a) and 9(b). Note that we take the half-width w of the incident beam larger than its wavelength λ_p ($w = 400\lambda_p$). It is found that when $\Omega_{41} = \Omega_{42} = R = 0, \gamma_{13} = 0.01\gamma$,, a large negative GH shift appears for the reflected beam, while the transmitted beam shows a small positive shift [Fig. 10(a)]. However, it is obvious from Fig. 10(b) that both the lateral shifts of the reflected and transmitted probe beams can be manipulated to be small positive by switching on the control field Ω_{42} ($\Omega_{42} = 8\gamma$), while keeping other parameters unchanged ($\Omega_{41} = R = 0$, $\gamma_{13} = 0.01\gamma$). These observations for the incident angle $\theta = 1.2$ rad are indeed analogous to the earlier results shown in Figs. 9(a) and 9(b), which admit a similar control on the lateral shifts. Therefore, our results remain valid for the real system. In order to further discuss the influence of w, we show in Fig. 11 the normalized intensity profiles for different half-width w with $\Omega_{41} = \Omega_{42} = 3\gamma$, $R = 0.2\gamma$, $\gamma_{13} = 0$, $\theta = 1.4$. It can be seen that for large width of the incident Gaussian field, the shapes of reflected and transmitted probe beams are very similar to the incident beam.

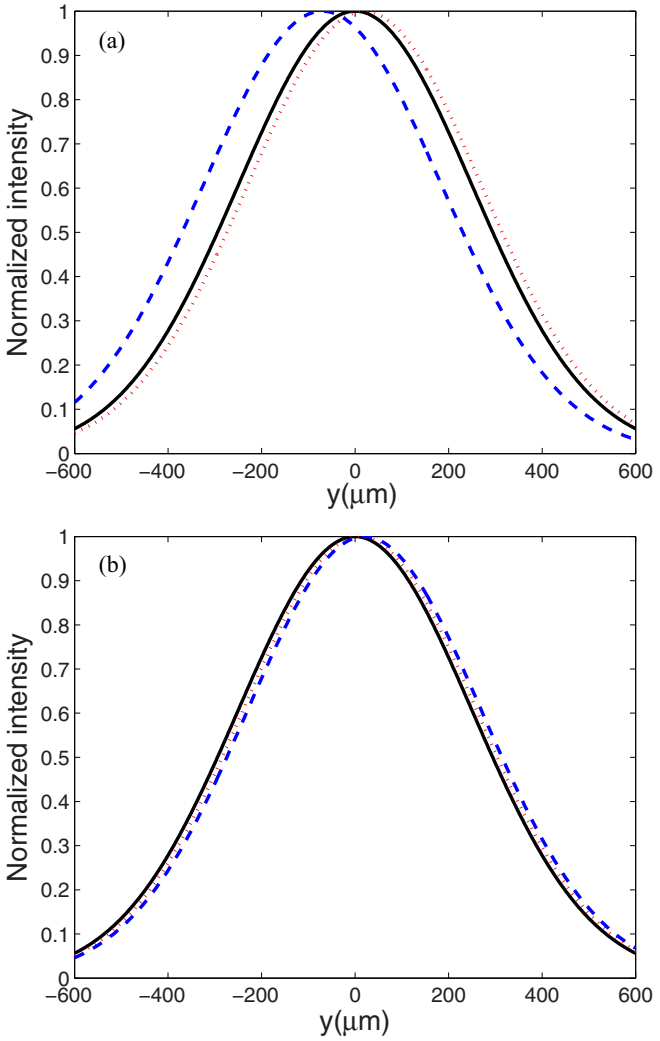

FIG. 10. (Color online) Plot of the normalized intensity profiles of the incident (solid line), reflected (dashed line), and transmitted (dotted line) probe beams for (a) $\Omega_{41} = \Omega_{42} = R = 0$, $\gamma_{13} = 0.01\gamma$, and (b) $\Omega_{42} = 8\gamma$, $\Omega_{41} = R = 0$, $\gamma_{13} = 0.01\gamma$. Here, $\theta = 1.2$, $w = 400\lambda_p$, and the rest of the parameters are the same as in Fig. 9.

V. CONCLUSIONS

A scheme of four-level mercury atomic medium is employed to realize the lateral shifts of a probe beam. It is found that (i) in the absence of the driving fields and without an incoherent pumping the medium experiences a strong absorption at zero probe field detuning for anomalous dispersion. In this case, we observe a negative GH shift in the reflected part of incident light, when the transmitted light undergoes positive GH shifts. When we take into account the influence of the driving fields, we observe significant different GH shift patterns; (ii) when only Ω_{42} is turned on, the reflected part of the incident beam captures the positive enhanced lateral shifts; (iii) when we include the effect of the second driving field Ω_{41}, negative shifts are observed in

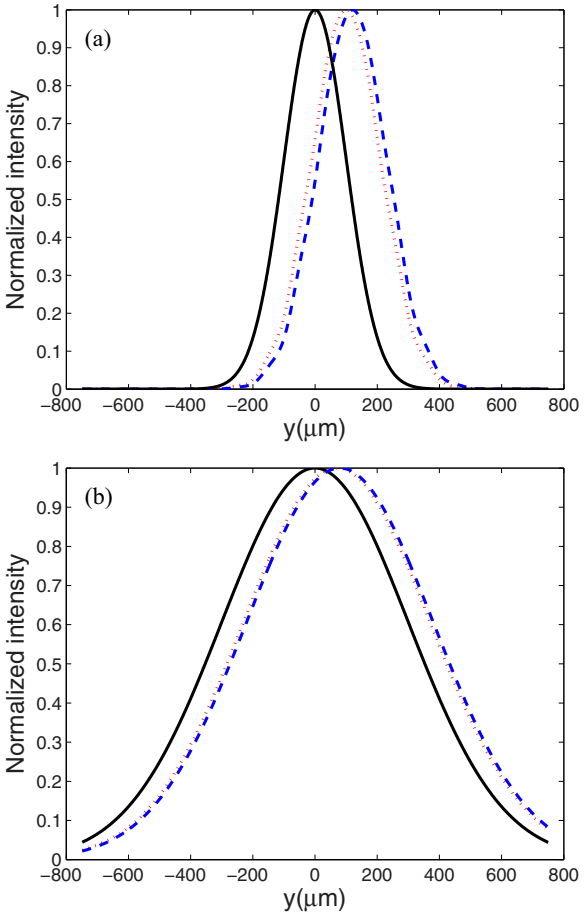

FIG. 11. (Color online) Plot of the normalized intensity profiles of the incident (solid line), reflected (dashed line), and transmitted (dotted line) probe beams for (a) $w = 100\lambda_p$ and (b) $w = 550\lambda_p$. Here, $\Omega_{41} = \Omega_{42} = 3\gamma$, $R = 0.2\gamma$, $\gamma_{13} = 0$,$\theta = 1.4$, and the rest of the parameters are the same as in Fig. 9.

S_r spectra. This special behavior is due to the interacting dark resonances which can be attributed to a high-resolution absorption peak and a very steep negative slope of dispersion in the susceptibility profile. However, it is realized that this defect is surmountable via applying a weak incoherent pump field (iv). Generalizing our study to the case of a VUV probe transition, the similar behavior with our earlier results of an UV probe transition case is observed. Finally, we showed that when the incident beam has a finite width, our previous results remain valid in the real system.

ACKNOWLEDGMENTS

The authors would like to announce their gratitude to the referee of the article for the fruitful comments, which significantly improved the paper. H.R.H. gratefully acknowledges the support of Lithuanian Research Council (Grant No. VP1-3.1-ŠMM-01-V-03-001). The authors would like to thank S. H. Asadpour for helpful discussion and simulation.

[1] Ying Wu, M. C. Chu, and P. T. Leung, Phys. Rev. A **59**, 3032 (1999).

[2] G. Juzeliūnas, J. Ruseckas, P. Öhberg, and M. Fleischhauer, Phys. Rev. A **73**, 025602 (2006); B. M. Anderson, I. B.

Spielman, and G. Juzeliūnas, Phys. Rev. Lett. **111**, 125301 (2013).
[3] H. Z. Shen, M. Qin, and X. X. Yi, Phys. Rev. A **88**, 033835 (2013); H. Z. Shen, M. Qin, Xiao-Ming Xiu, and X. X. Yi, *ibid.* **89**, 062113 (2014).
[4] S. M. Popoff, A. Goetschy, S. F. Liew, A. D. Stone, and H. Cao, Phys. Rev. Lett. **112**, 133903 (2014).
[5] R. W. Boyd and D. J. Gauthier, in *Slow and Fast Light, Progress in Optics*, Vol. 43, edited by E. Wolf (Elsevier, Amsterdam, 2002), Chap. 6, p.497.
[6] L. Thévenaz, Nat. Photonics **2**, 474 (2008).
[7] S. E. Harris, Phys. Today **50**(7), 36 (1997).
[8] Y. Wu and X. X. Yang, Phys. Rev. A **71**, 053806 (2005).
[9] J.-H. Li, X.-Y. Lü, J.-M. Luo, and Q.-J. Huang, Phys. Rev. A **74**, 035801 (2006).
[10] Z. Wang, A.-X. Chen, Y. Bai, W.-X. Yang, and R.-K. Lee, J. Opt. Soc. Am. B **29**, 2891 (2012).
[11] D.-c. Cheng, C.-p. Liu, and S.-q. Gong, Phys. Lett. A **332**, 244 (2004).
[12] H. R. Hamedi, Appl. Opt. **53**, 5391 (2014).
[13] A. Joshi, W. Yang, and M. Xiao, Phys. Rev. A **68**, 015806 (2003).
[14] Y. Niu and S. Gong, Phys. Rev. A **73**, 053811 (2006).
[15] W.-X. Yang, T.-T. Zha, and R.-K. Lee, Phys. Lett. A **374**, 355 (2009).
[16] Y. Wu and X. Yang, Appl. Phys. Lett. **91**, 094104 (2007).
[17] H. Sun, Y. Niu, S. Jin, and S. Gong, J. Phys. B: At. Mol. Opt. Phys. **41**, 065504 (2008).
[18] Y. Wu and X. Yang, Phys. Rev. B **76**, 054425 (2007).
[19] Y. Zhu, Phys. Rev. A **53**, 2742 (1996).
[20] L. Yuan, D. Wang, A. A. Svidzinsky, H. Xia, O. Kocharovskaya, A. Sokolov, G. R. Welch, S. Suckewer, and M. O. Scully, Phys. Rev. A **89**, 013814 (2014).
[21] M. O. Scully, Phys. Rev. Lett. **67**, 1855 (1991).
[22] T. Quang and H. Freedhoff, Phys. Rev. A **48**, 3216 (1993).
[23] G. S. Agarwal and S. Dasgupta, Phys. Rev. A **70**, 023802 (2004).
[24] F. Goos and H. Hänchen, Ann. Phys. (Leipzig, Ger.) **436**, 333 (1947); **440**, 251 (1949).
[25] H. K. V. Lotsch, Optik (Stuttgart, Ger.) **32**, 116 (1970); **32**, 189 (1970); **32**, 229 (1971); **32**, 553 (1971).
[26] T Hashimoto and T. Yoshino, Opt. Lett. **14**, 913 (1989).
[27] D. Felbacq, A. Moreau, and R. Smaâli, Opt. Lett. **28**, 1633 (2003).
[28] C.-F. Li, Phys. Rev. Lett. **91**, 133903 (2003).
[29] L. G. Wang, M. Ikram, and M. S. Zubairy, Phys. Rev. A **77**, 023811 (2008).
[30] Ziauddin, S. Qamar, and M. S. Zubairy, Phys. Rev. A **81**, 023821 (2010).
[31] W.-W. Deng, S.-P. Wu, and G.-X. Li, Opt. Commun. **285**, 2668 (2012).
[32] M. Rezaei and M. Sahrai, Eur. Phys. J. D **68**, 55 (2014).
[33] M. Abbas, Ziauddin, and S. Qamar, Laser Phys. Lett. **11**, 015201 (2014).
[34] Ziauddin and S. Qamar, Phys. Rev. A **84**, 053844 (2011).
[35] G. Xu, T. Zang, H. Mao, and T. Pan, Phys. Lett. A **374**, 3590 (2010).
[36] X. Chen, R.-R. Wei, M. Shen, Z.-F. Zhang, and C.-F. Li, Appl. Phys. B **101**, 283 (2010).
[37] Y Song, H.-C. Wu, and Y. Guo, Appl. Phys. Lett. **100**, 253116 (2012).
[38] Y. Wang, Y. Liu, and B. Wang, Phys. E **53**, 186 (2013).
[39] Z.-Z. Cao, Y.-F. Cheng, and G.-Q. Li, Phys. B **407**, 4254 (2012).
[40] M. Cheng, Eur. Phys. J. B **85**, 89 (2012).
[41] X. Chen, P.-L. Zhao, and X.-J. Lu, Eur. Phys. J. B **86**, 223 (2013).
[42] X. Chen, Y. Ban, and C.-F. Li, J. Appl. Phys. **105**, 093710 (2009).
[43] X. Chen, X.-J. Lu, Y. Wang, and C.-F. Li, Phys. Rev B **83**, 195409 (2011).
[44] P. T. Leung, C. W. Chen, and H.-P. Chiang, Opt. Commun. **276**, 206 (2007).
[45] F Pillon, H. Gilles, S. Girard, M. Laroche, R. Kaiser, and A. Gazibegovic, J. Opt. Soc. Am. B **22**, 1290 (2005).
[46] C. Luo, J. Guo, Q. Wang, Y. Xiang, and S. Wen, Opt. Express **21**, 10430 (2013).
[47] L.-G. Wang and S.-Y. Zhu, Opt. Lett. **31**, 101 (2006).
[48] J. Kuai and H. X. Da, J. Magn. Magn. Mater. **354**, 355 (2014).
[49] R. Yang, W. Zhu, and J. Li, Opt. Express **22**, 2043 (2014).
[50] M. Kumari and S. Dutta Gupta, Opt. Commun. **285**, 617 (2012).
[51] W. Löffler, M. P. van Exter, G. W. 't Hooft, E. R. Eliel, K. Hermans, D. J. Broer, and J. P. Woerdman, Opt. Commun. **283**, 3367 (2010).
[52] M.-W. Lu, X.-H. Huang, G.-L. Zhang, and S.-Y. Chen, Phys. Status Solidi B **249**, 2272 (2012).
[53] X. Chen, X.-J. Lu, Y. Ban, and C.-F. Li, J. Opt. **15**, 033001 (2013).
[54] E. S. Fry, M. D. Lukin, T. Walther, and G. R. Welch, Opt. Commun. **179**, 499 (2000).
[55] M. Mahmoudi, R. Fleischhaker, M. Sahrai, and J. Evers, J. Phys. B: At. Mol. Opt. Phys. **41**, 025504 (2008).
[56] L. G. Wang, H. Chen, and S. Y. Zhu, Opt. Lett. **30**, 2936 (2005).
[57] J. He, J. Yi, and S. He, Opt. Express **14**, 3024 (2006).
[58] D.-K. Qing and G. Chen, Opt. Lett. **29**, 872 (2004).
[59] X. Chen and C.-F. Li, Phys. Rev. E **69**, 066617 (2004).
[60] M. Cheng, Y. Zhou, Y. Li, and X. Li, J. Opt. Soc. Am. B **25**, 773 (2008).
[61] K. Artmann, Ann. Phys. **437**, 87 (1948); A. M. Steinberg and R. Y. Chiao, Phys. Rev. A **49**, 3283 (1994).
[62] Ziauddin and Sajid Qamar, Phys. Rev. A **85**, 055804 (2012); **87**, 029905(E) (2013); F. A. Hashmi and M. A. Bouchene, *ibid.* **88**, 047801 (2013); Ziauddin and S. Qamar, *ibid.* **88**, 047802 (2013).